Supplemental Data

Methods

Description of case cohorts

Summary data on the case cohorts studied are given in Supplementary Table 1. The UPenn cases were part of a cross-sectional study of Alzheimer disease (AD) pathology, whereas the ROS cases were part of a longitudinal epidemiological and clinico-pathological study of aging, including mild cognitive impairment (MCI) and AD. ROS cases are elderly Catholic clergy (nuns, priests, and brothers) non-demented at study entry who agree to annual clinical and neuropsychological evaluations with brain donation upon death. The follow-up rate for neuropsychological testing is above 95%, and the autopsy rate exceeds 90% (1,2). The subjects encompass a broad range of cognitive abilities and pathology, making the ROS cohort particularly useful for clinicopathological correlation analyses. Our cohort was selected randomly from the 350 deceased ROS subjects at the start this study. They did not differ significantly from the full set of ROS cases in age, sex ratios, PMIs, or last Mini-Mental State Examination (MMSE) scores within their diagnostic categories. There was no clear evidence of vascular damage in the cerebellar cortex or the hippocampal formation (HF) of any case studied.

Diagnoses

All cases of AD dementia studied met clinical criteria for that disorder specified by NINCDS-ADRA (3) as determined in consensus conferences after review of medical records, direct clinical assessments, and interviews of care providers. Clinical diagnosis requires that an individual showed clear cognitive decline from his or her previous levels as verified in tests of memory and in least one other cognitive domain (e.g., perceptual speed). The diagnoses were confirmed by postmortem examination of neuritic plaque densities in midfrontal gyrus (dorsolateral prefrontal cortex), superior + inferior temporal gyrus, inferior parietal gyrus, hippocampus, and substantia nigra as specified by the Consortium to Establish a Registry for AD (4). The final diagnoses were consistent with Braak scores for neurofibrillary tangle (NFT) pathology as recommended by the NIA-Reagan Institute consensus on diagnosis of AD (5).

Diagnosis of MCI (6,7) was purely clinical and indicates that an individual was rated at the last examination as cognitively impaired according to neuropsychological tests but not demented according to the examining physician (1). A diagnosis of amnestic MCI (aMCI) indicates that the individual displayed prominent deficits in episodic memory at the final evaluation. As this implies, a diagnosis of non-amnestic MCI (naMCI) indicates that the individual displayed predominant cognitive deficits other than memory (i.e., perceptual speed and/or visuospatial ability) at the last evaluation.

Cognitive Testing

Yearly evaluations of the ROS subjects include neuropsychological testing, as well as completion of a medical history, neurological examination, and ratings on psychiatric scales. The average time between the last neuropsychological evaluation and death is 6-7 months. As previously described (8,9), such evaluation included the MMSE and 7 tests of episodic memory, 4 of semantic memory, 4 of working memory, 2 of perceptual speed, and 2 of visuospatial ability. A subject's test results from the annual exam closest to death were used. For data reduction in each subject, raw scores on individual tests were converted to *z* scores relative to the baseline mean and standard deviation for the entire ROS cohort. These were averaged to yield composite scores on the cognitive domains noted above (e.g., episodic memory), which were in turn averaged to yield a composite global cognition score.

Tissue Collection

Autopsy consent was obtained from the brain donors, next-of-kin, or legal guardians in all cases. Postmortem cases were stored at 2-4°C until autopsy. After sagittal bisection of the forebrain, the brain was cut into coronal slabs. One hemisphere was sampled for tissues to be examined microscopically, including the cerebellar cortex, HF, and other brain areas used for diagnostic neuropathological assessments indicated above. Samples were fixed in neutral-buffered formalin for 24-48 h, and embedded in paraffin. Undissected tissue was frozen overnight at -80°C and sealed in plastic bags for long-term storage at the same temperature. Cerebellar cortex and HF tissue were later dissected from the frozen hemispheres of 8 matched pairs of normal and AD cases for the ex vivo stimulation with insulin as described below. Surfaces were shaved before thawing to remove oxidized surfaces.

Anatomical origin and laminar content of samples

Cerebellar cortex samples derived from the midline of the posterior cerebellar lobe. Human HF samples derived from mid-coronal levels of that structure. Rat HF samples included the full rostrocaudal extent of that structure. Tissue samples included all layers and cell types of the structure studied (molecular, Purkinje, and granule cell layers of the cerebellar cortex; molecular, granule cell, and polymorph layer of the dentate gyrus; lacunosum-molecular, radiate, pyramidal, and oriens layers of the hippocampus; and molecular and pyramidal cell layers of the subiculum).

Histological preparations

Formalin-fixed, paraffin-embedded blocks of dissected brain areas were sectioned at 6 μm, mounted on APES-coated slides (10), and air dried. The sections sampled intermediate rostrocaudal levels of the HF. After dewaxing and rehydration, the tissue was either stained for Nissl substance or prepared for immunohistochemistry. To delineate cytoarchitectural limits of HF cell fields and estimate cell loss in AD cases, adjacent sections were stained in 0.1% cresyl violet acetate (Acros Organics 229630050, Fisher Scientific) at (pH 4.3), differentiated in 95% ethanol, dehydrated in 100% ethanol, cleared in xylenes, and coverslipped under Cytoseal 60 (Fisher Scientific). Since it was necessary to determine the maximum size of cell nuclei to selectively identify cells with extranuclear immunoreactivity, a third set of HF sections was stained with the nuclear marker hematoxylin. Sections were first stained with Gill 3 hematoxylin (Polysciences 24244) for 2 min, rinsed in running tap water for 1 min, then soaked in Scott's bluing reagent (StatLab SL99) for 2 min, rinsed again in running tap water for 1 min, dehydrated in ascending concentrations of ethanol, cleared in xylenes, and coverslipped under Cytoseal 60.

Neuropathological examination

All cases were fully examined by trained neuropathologists for gross and microscopic abnormalities diagnostic of diverse neurodegenerative dementias. Gross examination was performed at autopsy, after which microscopic inspection was performed on fixed 6 μm sections in multiple brain areas specified above (see ***Diagnoses***). Hematoxylin and eosin staining was used to reveal cell loss and infarcts not seen on gross examination. Neuritic plaques were visualized with NAB228 (1:5000), a mouse monoclonal raised against $A\beta_{1\text{-}11}$ synthetic peptide (Santa Cruz Biotechnology 32277). Neurofibrillary tangles (NFTs) were

visualized using AT8 (1:800), a mouse monoclonal to hyperphosphorylated tau for neurofibrillary tangles (Thermo Fisher). Aβ plaque load and NFT density were quantified with the image analysis using procedures described below for other immunohistochemical tests.

Quantitative immunohistochemistry

Tissue sections were first dewaxed in xylenes, rehydrated in descending alcohols, and quenched of endogenous peroxidase activity in 5% H_2O_2 dissolved in methanol for 30 min. They were then were rinsed in distilled water and treated with an epitope retrieval method. The retrieval treatment (formic acid denaturation, boiling, or trypsin digestion) depended on the antigen studied. For Aβ and phosphorylated tau, sections were immersed for 10 min in concentrated formic acid (Fisher Scientific BP1215-500) similar to the method of Kitamoto et al. (11). For IR/IGF-1β pY and IRβ Y^{960}, sections were incubated on-the-slide for 20 min at 37°C in dissolved trypsin tablets with buffer salts (Sigma-Aldrich T-7168). For all other antigens, sections were boiled for 10 min in 10 nM citrate (pH 6.0) or, much more commonly, 1 mM EDTA (pH 8.0) as advocated by Pileri et al. (12).

After antigen retrieval treatment, the tissue was rinsed in water, transferred to 0.1 M Tris buffer with 0.01% Triton X-100 (TTB), blocked in 10% normal horse serum, and incubated in primary antibody overnight at 4°C. Primary antibodies and their concentrations are given in Supplementary Table 7. After rinsing in TTB and again between steps, sections were incubated in species-appropriate biotinylated secondary antibody for 1 h at room temperature, transferred to an avidin-biotin-peroxidase complex for 1 h, and finally reacted with a 0.05% diaminobenzidine (DAB) – 0.03% hydrogen peroxide solution for 10 min. For most antigens, signal amplification was achieved by adding $NiSO_4$ (0.25% final dilution) to the DAB solution (13). For PIP3, the DAB reaction product was darkened by light silver-gold intensification following Teclemariam-Mesbah et al. (14). For Akt, Akt1 pS^{473}, Akt2 pS^{474}, and PTEN, the IHC protocol was modified according to the protocol of Soetanto et al. (15) to permit tyramide signal amplification (TSA) of streptavidin-peroxidase mediated DAB reaction product using the TSA Biotin System (NEL700) of Perkin Elmer. Sections were then rinsed in water, dehydrated in ascending concentrations of alcohols, cleared in xylenes, and coverslipped under Cytoseal 60. All antigens were studied in at least two independent sets of normal and AD cases.

Measurement of cytoplasmic antigen levels

Quantifying differences between AD and normal cases in cytoplasmic levels of antigens of interest was complicated by the fact that in the controls some of the antigens were only reliably detected, if at all, in cell nuclei even after antigen retrieval and signal amplification (Figure 6 G, M and Supplemental Figures 5 G, J, M and 6 D, G, J). We consequently used two measures of cytoplasmic antigen levels. When an antigen *in normal cases* was commonly detected in cytoplasm, but not in nuclei (AS160 pT^{642}, GLUT4 pS^{488}, GSK-3β, GSK-3α/β $pS^{21/9}$, IRβ, IRβ pY^{960}, IR/IGF-1Rβ pY, total IRS-1, PP2A, PP2B, PTEN, and PTP1B), we used mean cell body immunoreactivity (optical density) as the measure of cytoplasmic levels. But when an antigen *in normal cases* was often undetectable in cytoplasm or cell nuclei (Akt1, Akt2, and nitrotyrosine) or was heavily concentrated in (or restricted to) cell nuclei (PIP3 and phosphorylated Akt, JNK, IKK, IRS-1, PKCζ/λ, and mTOR), we used the density of cell bodies with detectable cytoplasmic antigen (immunoreactive cells per unit area, normalized to total neuron density) as an index of cytoplasmic antigen levels. Use of this index in CA1 gave results qualitatively similar to, but larger than, total antigen levels in Western blotting of the HF as a whole, which includes areas (i.e., CA3 and dentate gyrus) displaying much less pathology and insulin signaling abnormalities in AD.

(Supplemental figures on the following pages)

Supplemental Figures

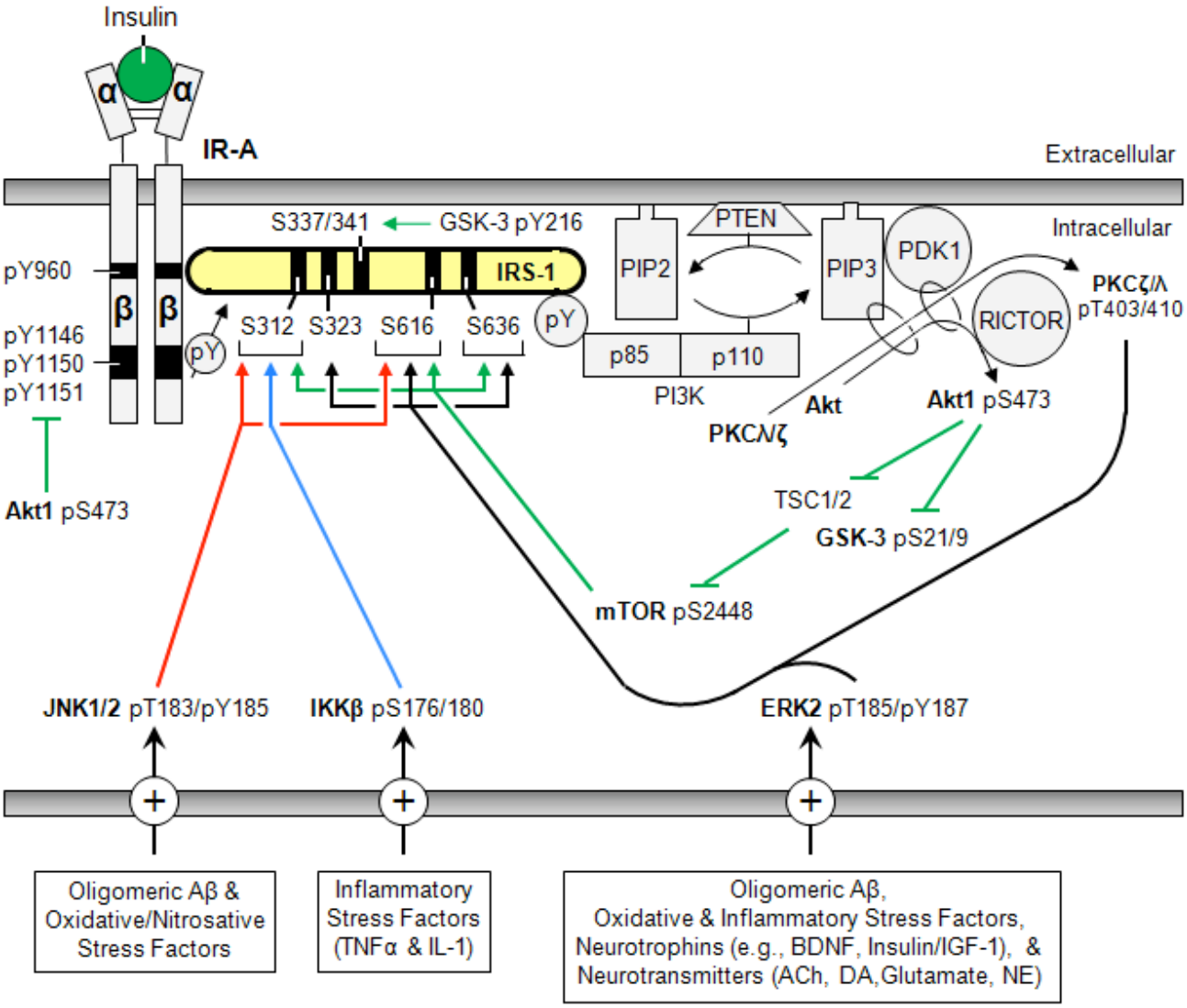

Supplemental Figure 1: Schematic of the insulin signaling pathway whose disruption causes insulin resistance in T2D (16-20). The insulin receptor (IR) has two extracellular α chains and two transmembrane β chains. Only the IR with abbreviated α chains (IR-A) exists in the brain (21-24). Insulin binding of the IR α chains activates autophosphorylation of the β chains, resulting first in tyrosine phosphorylation (pY) of amino acids 1146, 1150, and 1151 in the catalytic (kinase regulatory) domain (= Y1158, 1162, and 1163 in full-length IR called IR-B) and later in tyrosine phosphorylation of amino acid 960 (= Y972 in IR-B). The latter event promotes IR binding of insulin receptor substrates (IRSs) (25,26). IRS-1, but not IRS-2, is shown since only the former is recruited to brain IRs by near physiological doses of

insulin according to the present study. IRS-1 pY binds the p85 regulatory subunit of phosphatidylinositol 3-kinase (PI3K), which catalyzes the conversion of PIP2 to PIP3. The latter phospholipid promotes translocation of protein kinase B (Akt) and protein kinase C, including PKC isoforms zeta [ζ] and lamba [λ], to the cell membrane, where they are activated via the kinases PDK1 and/or Rictor (27,28). Via interactions with Grb2 (not shown), IRS-1 can also activate ERK (25,26,29). Akt1 activation exerts feedback inhibition on IRβ directly (30) and on IRS-1 indirectly via the mammalian target of rapamycin (mTOR) (31,32). Direct feedback inhibition of IRS-1 is exerted not only by mTOR, but also by other serine kinases, including ERK2, GSK-3, and PKCζ/λ phosphorylating IRS-1 at S312, S323, S337/341, S616, and S636 numbered according to the human amino acid sequence: cf. refs. (17,31,33-36). Those sites in rodents are respectively S307, S318, S332/336, S612, and S632 (31). Via ERK2, JNK 1+2, and IKKβ, many extracellular factors specified in the diagram can also inhibit IRS-1 (18,31,37,38). Apart from the serine phosphorylated forms of IRS-1 and GSK, all the phosphospecific molecules shown are their activated forms.

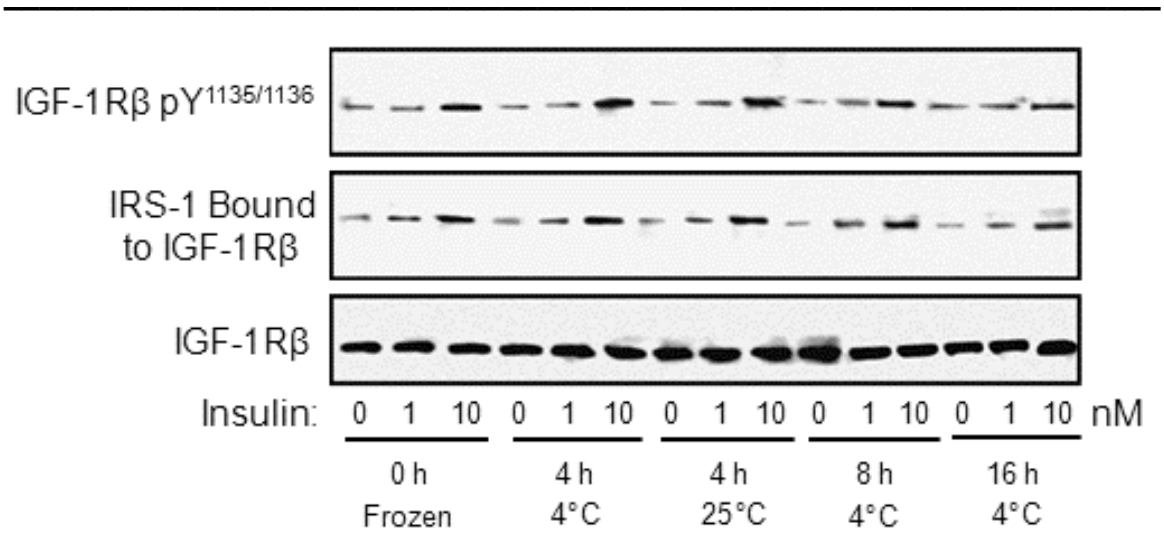

Supplemental Figure 2: Postmortem intervals up to 16 h between death and brain removal do not affect the magnitude of signaling responses to ex vivo insulin stimulation in the rat HF. As confirmed by quantitative analyses, these representative immunoblots show that 10 nM, but not 1 nM, insulin consistently increases IGF-1R activation and recruitment of IRS-1. Text Figure 1C and D graphs such data from all the rat brains studied.

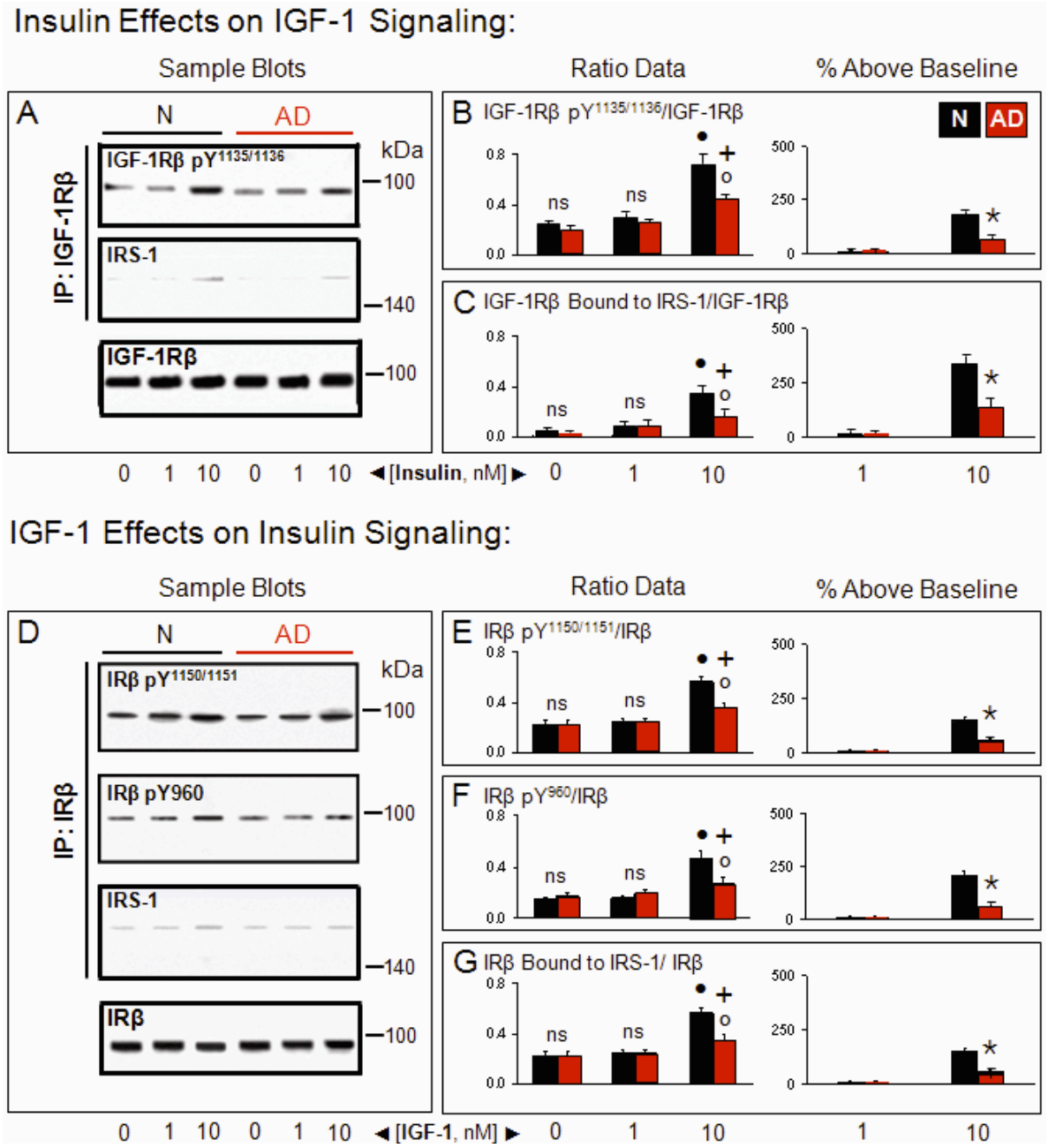

Supplemental Figure 3: Near-physiological doses of insulin and IGF-1 (1 nM) selectively activate their cognate receptors in normal (N) human and AD brains. The HF from the 8 matched pairs of normal and AD cases described in the text was stimulated ex vivo with insulin (**A**-**C**) or IGF-1 (**D**-**G**). Sample immunoblots from a representative matched pair of cases are shown. The 1 nM insulin dose did not affect levels of IGF-1Rβ $pY^{1135/1136}$ in the catalytic domain of that receptor or IGF-1Rβ binding of IRS-1 as seen in ratio measurements (mean ratio ± SEM) and the percentage increase above baseline levels (mean ratio ± SEM) in these signaling responses. Conversely, 1 nM IGF-1 had no significant effect on IRβ $pY^{1150/1151}$ in the receptor's catalytic domain), IRβ pY^{960} in the receptor's IRS-1

binding domain, or IRβ binding of IRS-1. In contrast, 10 nM doses of either ligand activated the IR plus IGF-1R. The results are quantified in text Tables 2 and 4 and Supplemental Tables 3A and 5. ns = not significant, ○ and ● = $p < 0.05$ and $p < 0.01$, respectively, for differences from baseline levels in the same diagnostic group, and ✶ and ✚ = $p \leq 0.01$ and $p < 0.005$, respectively, for differences between diagnostic groups.

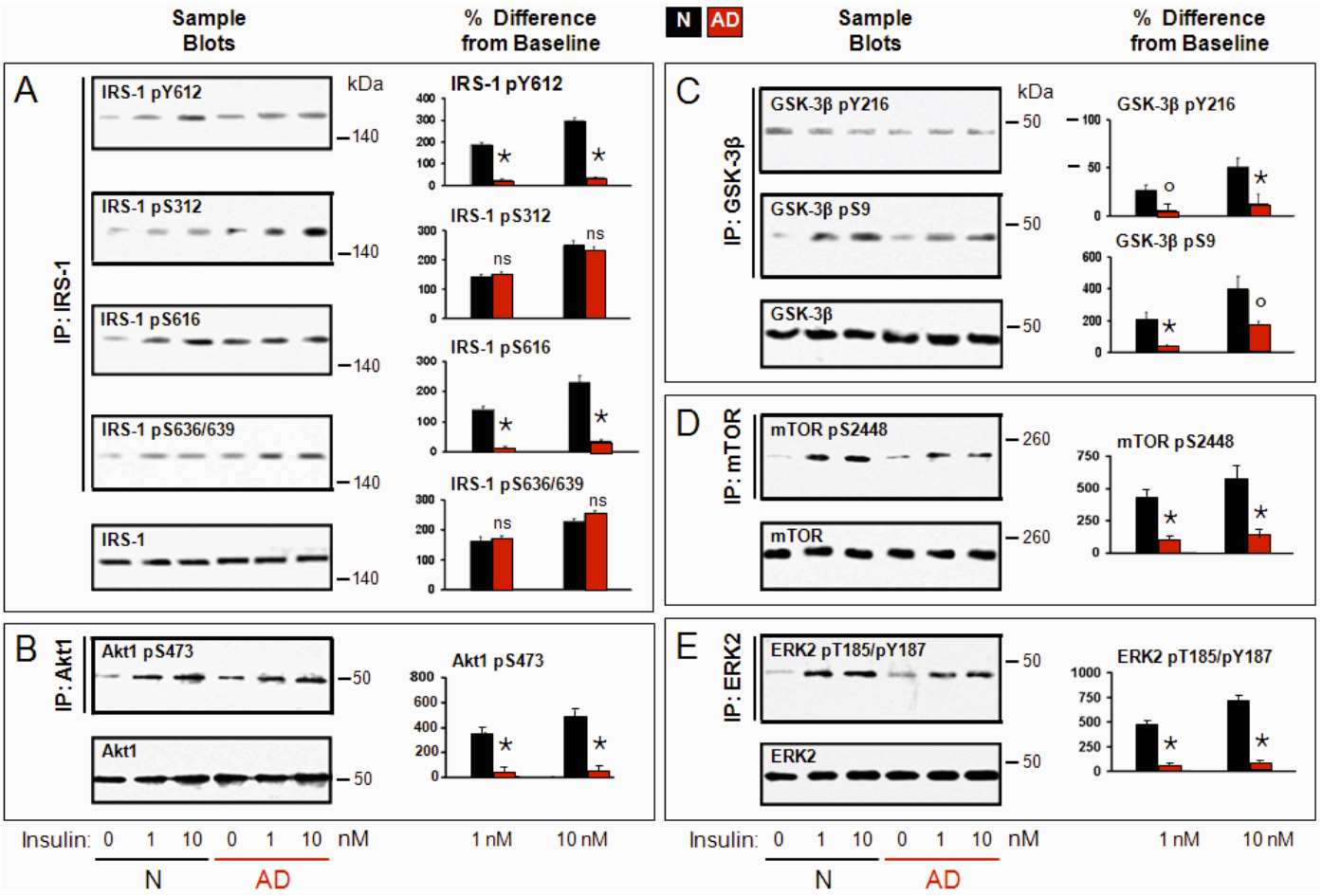

Supplemental Figure 4: HF insulin signaling responses in normal (N) and AD cases not illustrated in the text. Tissue from the 8 matched pairs of normal and AD cases described in the text was tested ex vivo. Sample immunoblots from a representative matched pair are shown. Responses are expressed as percentages of baseline (0 nM) levels (mean ratio ± SEM) in the same diagnostic group, all of which are percent increases except for GSK-3β pY^{216} expressed in percent decreases. The statistical significance of differences between N and AD cases is indicated: ns = not significant, ○ = $p < 0.05$, ✶ = $p < 0.005$. For quantification of results, see text Table 2.

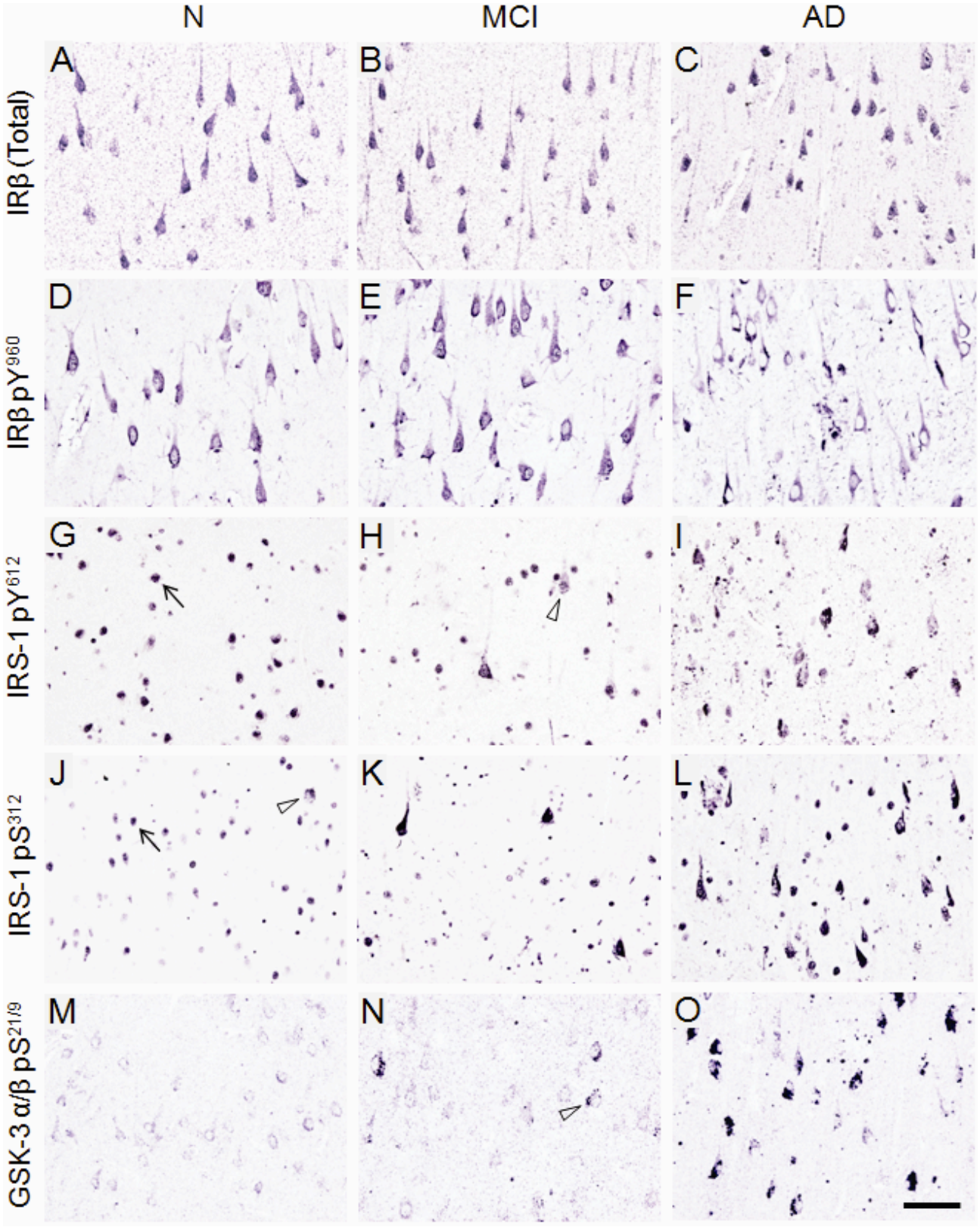

Supplemental Figure 5 (Figure legend on next page)

Supplemental Figure 5 (above)**:** IRβ (**A**-**C**), IRβ pY^{969} (**D**-**F**), IRS-1 pY^{612} (**G**-**I**), IRS-1 pS^{312} (**J**-**L**), and GSK-3 α/β pS$^{21/9}$ (**M**-**O**) seen immunohistochemically in CA1 neurons of normal (N), mild cognitive impairment (MCI), and AD cases in the ROS cohort. Text Table 5 summarizes the numeric data on these antigens. Unlike IR/IGF-1Rβ pY, IRβ pY^{960} was not reduced in MCI, but both these IRβ pY species were reduced in AD. Activated forms of IRS-1 (IRS-1 pY^{612} and IRS-1 pY^{941}), like IRS-1 pS, were often confined to cell nuclei in normal cases (e.g., arrows in **G** and **J**). An example of a rare exception is indicated by an arrow head in panel **J**. Cytoplasmic IRS-1 pY^{612} and IRS-1 pS^{312}, was seen more commonly in MCI (e.g., arrowhead in **H**), but the increase in density of neurons with these antigen in cytoplasm was significant only between N or MCI cases and AD cases, not between N and MCI cases. (Human IRS-1 pY^{612} and pY^{941} = rodent IRS-1 pY^{608} and pY^{939}, respectively). GSK-3α/β pS$^{21/9}$ was cytoplasmic and its levels rose slightly (e.g., arrow head in **N**), but insignificantly, in MCI cases and very significantly in AD (see text Table 5). The scale bar in **O** is 70 μm and applies to all panels.

Supplemental Figure 6 (below)**:** Other IRS-1 pS kinases (**A**-**L**) and nitrotyrosine (**M**-**O**) seen immunohistochemically in CA1 neurons of normal (N), mild cognitive impairment (MCI), and AD cases in the ROS cohort. Text Table 5 summarizes the numeric data on the antigens shown. Nitrotyrosine was cytoplasmic with low levels in N cases that rose significantly in MCI cases and again in AD cases. A different pattern of changes were noted for the other antigens, all known to phosphorylate the IRS-1 pS sites studied here. In N cases, activated IKKα/β (pS$^{176/180}$), JNK (pT^{183}/pY^{185}), mTOR (pS^{2448}), and PKCζ/λ (pT$^{410/403}$) were frequently confined to cell nuclei (e.g., arrows in **A**, **D**, **G**, and **J**). In MCI and again in AD, the density of cells with detectable levels of activated, cytoplasmic IKK, JNK, mTOR, and PKCζ/λ (e.g., arrow heads in **B**, **E**, **H**, **K**, and **N**) increased, though the increase was significant only in AD cases (see text Table 5). The density of neurons with cytoplasmic IRS-1 pS was highly correlated with the density of neurons expressing activated, cytoplasmic mTOR, IKK, and PKCζ/λ (see text Table 6). The scale bar in **O** is 70 μm and applies to all panels.

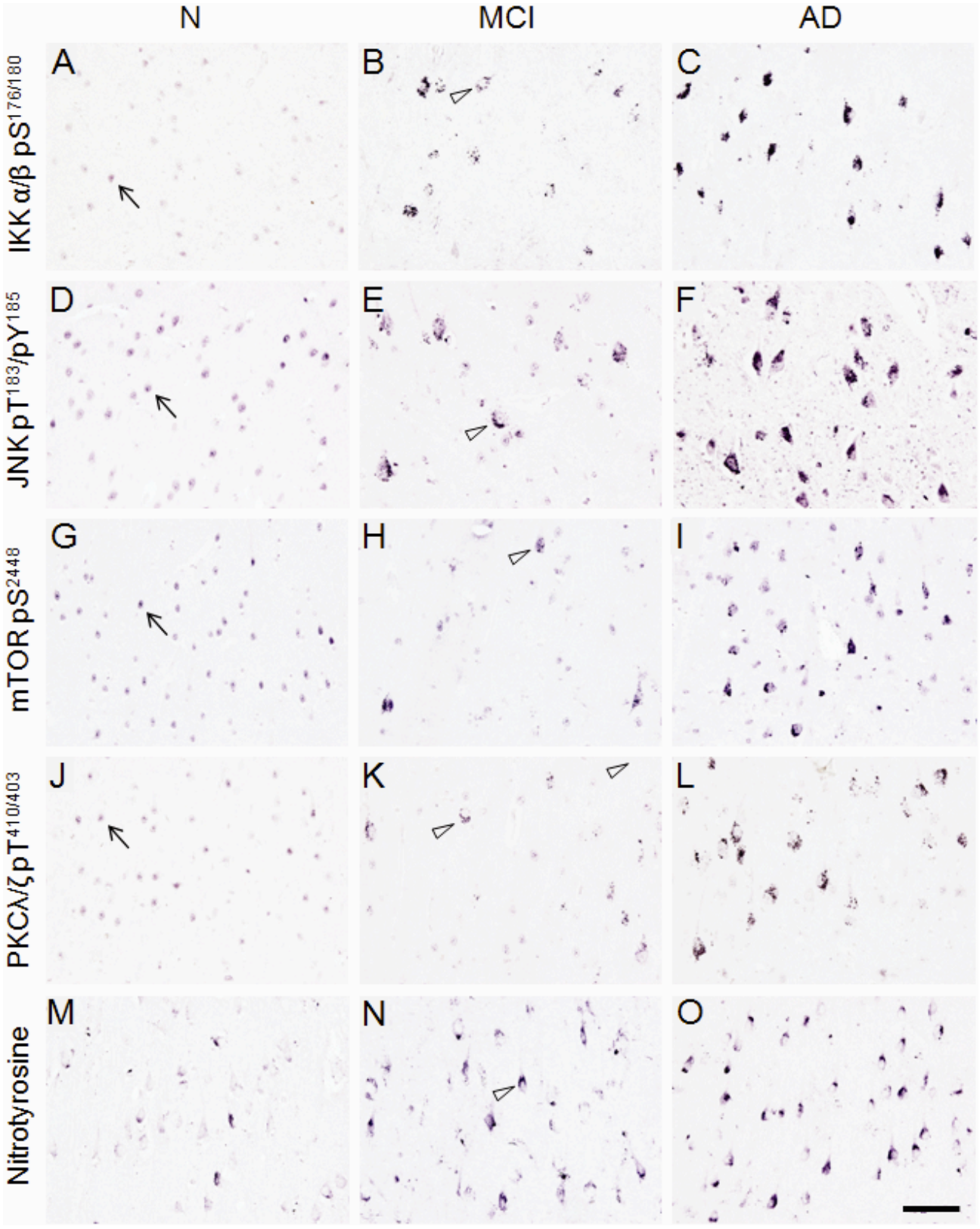

Supplemental Figure 6 (Figure legend on preceding page)

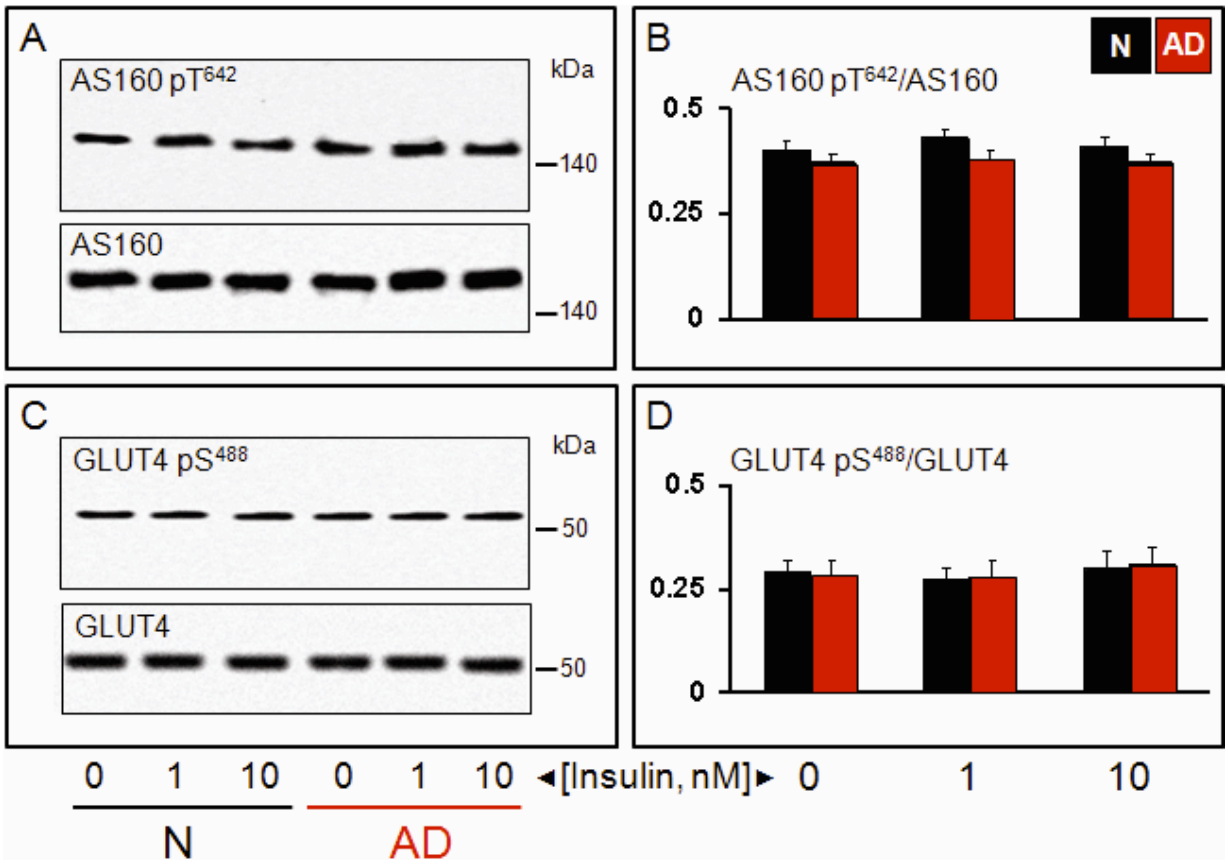

Supplemental Figure 7: Insulin by itself does not affect levels of the glucose uptake markers AS160 pT^{642} and glucose transporter 4 (GLUT4) pS^{488} in the HF of normal or AD cases. Ex vivo tests were run on the 8 pairs of normal (N) and AD cases studied for insulin resistance. AS160 pT^{642} (**A** and **B**) and GLUT pS^{488} (**C** and **D**) were measured in immunoprecipitated AS160 and GLUT4, respectively. Total AS160 and GLUT4 in N and AD cases did not differ significantly, as indicated at 0 nM insulin ($p = 0.1877$ and 0.7141, respectively). Nor were there significant differences in basal AS160 pT^{642} and GLUT pS^{488} between N and AD cases ($p = 0.1649$ and 0.9140, respectively). As apparent in **C** and **D**, insulin at 1 or 10 nM had no effect on levels of AS160 pT^{642} or GLUT pS^{488} in N cases ($p > 0.29$) or AD cases ($p > 0.10$). There were thus no differences between N and AD cases in insulin-induced levels of glucose uptake markers ($p = 0.1649$ for AS160 pT^{642} and $p = 0.9140$ for GLUT4 pS^{488}).

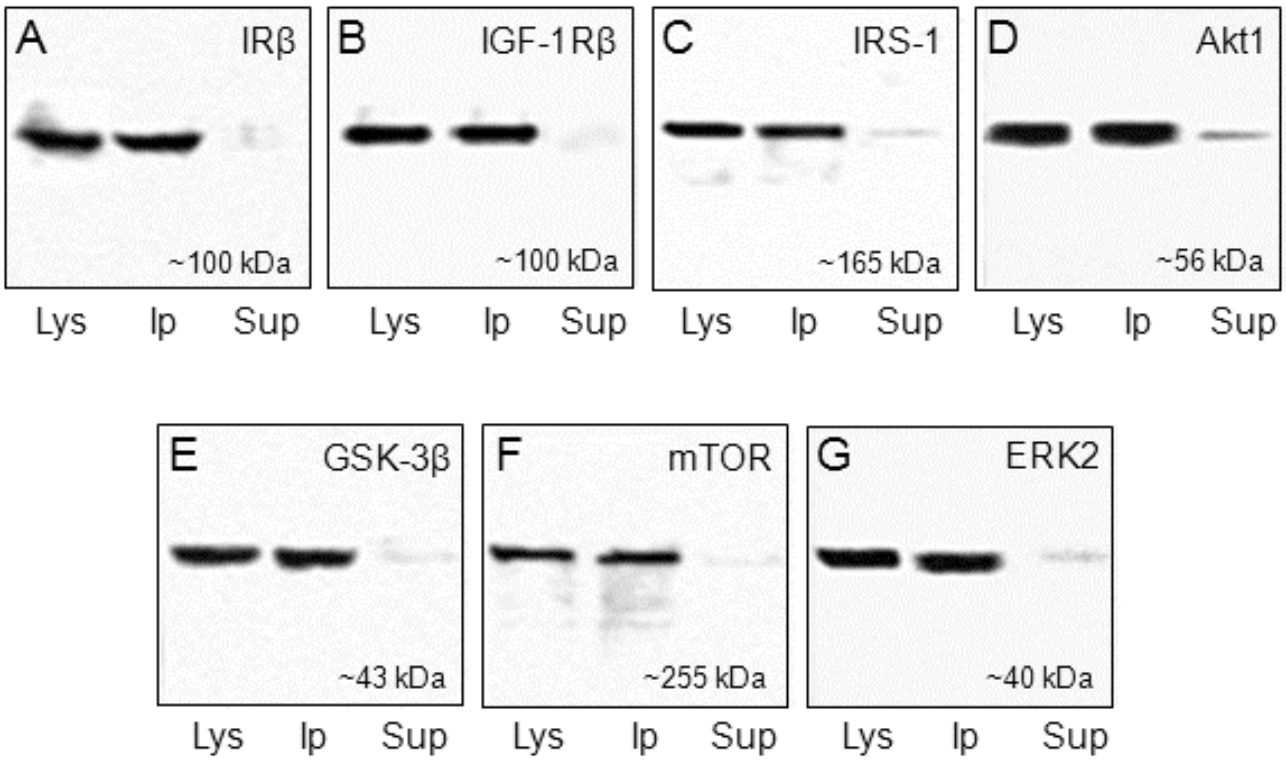

Supplemental Figure 8: Representative Western blots verifying completeness of immunoprecipitation for the HF proteins studied: IRβ (**A**), IGF-1β (**B**), IRS-1 (**C**), Akt1 (**D**), GSK-3β (**E**), mTOR (**F**), and ERK2 (**G**). Three normal HF with the highest antigen levels among 8 fresh frozen samples were chosen for testing. Results are shown for one of three samples. The lanes in each blot show relative amount of antigen in the tissue lysate (Lys), the immunoprecipitate (Ip) of that lysate, and the remaining supernatant (Sup). As the supernatants show, at least 90% of each antigen was immunoprecipitated. The approximate molecular weight of the bands shown are given in the lower right corner of each blot.

(Supplemental tables on following pages)

Supplemental Table 1

Characterization of cohorts studied[A]

	UPenn		ROS		
Variable	***N***	***AD***	***N***	***MCI***	***AD***
Number of cases	24	24	30	29	31
Age (y, m ± SD)	72.58 ± 13.2	73.92 ± 11.1	84.38 ± 6.0	87.70 ± 5.7	88.04 ± 5.5
Age range (y)	47-93	51-89	71-96	76-101	76-100
Sex ratio (males/females)	11m/13f	11m/13f	15m/15f	11m/18f	15m/16f
Caucasian/non-Caucasian [B]	18/6	18/6	30/0	15/2	31/0
Cases with history of T2D	0	0	6	1	7
Education (y, m ± SD)	NA[C]	NA	19.43 ± 2.6	18.38 ± 3.3	17.32 ± 3.4
MMSE score (m ± SD)	NA	NA	28.33 ± 1.1	26.86 ± 2.5†	16.68 ± 0.7●
Global cognition Index[D] *(m ± SD)*	NA	NA	0.006 ± 0.3	– 0.527 ± 0.3§	– 1.763 ± 0.9●
Episodic memory Index[D] *(m ± SD)*	NA	NA	0.319 ± 0.4	– 0.467 ± 0.5§	– 2.28 ± 1.1●
Working memory Index[D] *(m ± SD)*	NA	NA	– 0.075 ± 0.5	– 0.347 ± 0.5†	– 1.337 ± 1.0●
Postmortem interval (h, m ± SD)	11.98 ± 5.1	9.48 ± 4.0	6.20 ± 4.3	7.22 ± 6.4	6.14 ± 4.8
Braak stage (m ± SD)	1.84 ± 1.0	4.56 ± 0.8Δ	2.87 ± 1.2	3.55 ± 1.0[E]	4.13 ± 1.2Δ
CA1 NFT density (cells/mm², m ± SD)	4.29 ± 6.8	33.8 ± 13.5Δ	1.86 ± 3.8	1.99 ± 3.8†	11.47 ± 11.6●
CA1 total Aβ plaque load with NAB228 (m ± SD) [F]	0.148 ± 0.3	2.68 ± 1.6Δ	0.128 ± 0.3	0.243 ± 0.5	0.450 ± 0.5Δ
CA1 oligomeric Aβ plaque load with NU-4 (m ± SD) [G]	0.078 ± 0.1	1.24 ± 0.8Δ	0.239 ± 0.5	0.326 ± 0.5†	0.757 ± 0.7●
CA1 neuron density (cells/mm², m ± SD) [H]	67.70 ± 18.1	44.36 ± 16.2Δ	107.90 ± 33.3	113.5 ± 34.9†	73.55 ± 36.5●
CA1 neuron size (um², m ± SD) [H]	577.0 ± 104.3	529.0 ± 61.4	507.8 ± 181.4	426.8 ± 116.1	399.8 ± 144.3Δ

[A] AD = Alzheimer's disease, MCI = mild cognitive impairment, N = normal, not cognitively impaired, MMSE = mini-mental state exam, m ± SD = mean ± standard deviation. The MCI group included 12 amnestic and 17 non-amnestic cases

[B] The non-Caucasians in the UPenn cohort were 2 male and 4 female African-American NCI cases. The non-Caucasians in the ROS cohort were non-amnestic MCI cases: an African-American female and a Vietnamese male.

[C] Data on years of education and quantified cognitive status proximal to death are not routinely available (NA) on the UPenn cases.

[D] Composite score based on multiple cognitive tests (4).

[E] Compared to normal cases, Braak scores were significantly elevated in amnestic MCI (m ± SD, 4.0 ± 0.8), but not in non-amnestic MCI (m ± SD, 3.23 ± 1.0) cases.

[F] Aβ plaque load is defined as the percent of CA1 cross sectional area covered by Aβ plaques.

[G] Similar results were obtained with two oligomeric Aβ antibodies (NU-1 and NAB61).

[H] Based on Nissl data.

Superscript symbols indicate significant differences ($p < 0.05$) from NCI (Δ), from AD (†), from N and MCI (●), and from N and AD (§).Within the UPenn samples and within the ROS samples, groups did not differ significantly in age or PMI.

Supplemental Table 2

Basal and insulin-stimulated levels of signaling molecules and their interactions in cerebellar cortex of normal (N) and AD cases[A]

Signaling molecule ratios	0 nM Insulin (Basal Levels)			1 nM Insulin			10 nM Insulin		
	N	AD	N vs. AD *P* Value	N	AD	N vs. AD *P* Value	N	AD	N vs. AD *P* Value
IR									
IR $pY^{1150/1151}$/ IR	0.13 ± 0.01	0.13 ± 0.01	0.74051	0.46 ± 0.04	0.36 ± 0.03	0.04122	0.59 ± 0.03	0.51 ± 0.04	0.14993
IR pY^{960}/ IR	0.16 ± 0.02	0.20 ± 0.03	0.26028	0.54 ± 0.06	0.35 ± 0.03	0.00859	0.61 ± 0.04	0.51 ± 0.05	0.11652
IRS-1									
Total IRS-1 pY/ IRS-1	0.09 ± 0.01	0.10 ± 0.02	0.62644	0.32 ± 0.03	0.24 ± 0.03	0.02367	0.41 ± 0.03	0.34 ± 0.04	0.11466
IRS-1 pY^{612}/ IRS-1	0.19 ± 0.02	0.20 ± 0.02	0.69283	0.54 ± 0.07	0.33 ± 0.06	0.02269	0.67 ± 0.07	0.58 ± 0.05	0.29271
Total IRS-1 pS/ IRS-1	0.16 ± 0.02	0.18 ± 0.02	0.12290	0.41 ± 0.04	0.29 ± 0.03	0.01334	0.50 ± 0.04	0.37 ± 0.03	0.00034
IRS-1 pS^{312}/ IRS-1	0.14 ± 0.02	0.15 ± 0.02	0.65023	0.45 ± 0.04	0.39 ± 0.03	0.63242	0.50 ± 0.01	0.47 ± 0.03	0.51973
IRS-1 pS^{616}/ IRS-1	0.09 ± 0.01	0.13 ± 0.01	0.00321	0.26 ± 0.05	0.21 ± 0.02	0.26991	0.38 ± 0.07	0.31 ± 0.04	0.36324
IRS-1 $pS^{636/639}$/ IRS-1	0.13 ± 0.01	0.23 ± 0.02	<0.00001	0.40 ± 0.03	0.28 ± 0.03	0.00034	0.48 ± 0.04	0.35 ± 0.03	0.00070
IRS-1 interactions									
IRS-1 bound to IRβ/ IRβ	0.05 ± 0.01	0.05 ± 0.01	0.31452	0.27 ± 0.03	0.19 ± 0.01	0.02273	0.36 ± 0.03	0.25 ± 0.03	0.01831
PI3K p85α bound to IRS-1/ IRS-1	0.15 ± 0.01	0.20 ± 0.02	0.00672	0.38 ± 0.05	0.28 ± 0.03	0.05893	0.56 ± 0.04	0.46 ± 0.05	0.25047
IRS-2									
Total IRS-2 pY/ IRS-2	0.16 ± 0.02	0.18 ± 0.02	0.41354	0.19 ± 0.02	0.19 ± 0.02	0.71955	0.28 ± 0.02	0.22 ± 0.01	0.09133
Total IRS-2 pS/ IRS-2	0.21 ± 0.02	0.34 ± 0.03	0.00102	0.24 ± 0.02	0.36 ± 0.03	0.02997[B]	0.31 ± 0.02	0.37 ± 0.03	0.06509
IRS-2 interactions									
IRS-2 bound to IRβ/ IRβ	0.03 ± 0.01	0.03 ± 0.01	0.35799	0.03 ± 0.01	0.03 ± 0.02	0.24453	0.04 ± 0.02	0.05 ± 0.02	0.11155
PI3K p85α bound to IRS-2/ IRS-2	0.24 ± 0.02	0.24 ± 0.02	0.87813	0.25 ± 0.02	0.25 ± 0.02	0.68839	0.40 ± 0.03	0.28 ± 0.02	0.00011

[A]Data expressed as ratios (mean ± S.E.M) of signaling molecules listed at left, either levels of a phosphorylated molecule to total levels of that molecule or levels of a bound molecule to total levels of the molecule to which it is bound. 1 nM insulin selectively activates the IR, but 10 nM insulin activates the IR and IGF-1R (see text Figures 1 and 2 and Supplemental Figures 2 and 3).

[B]Although there were significant between-groups (N vs. AD) effects on levels of IRS-2 pS at 1 nM insulin, that dose did not significantly increase values above baseline levels within either diagnostic group. The between-groups effect thus appears to reflect differences between N and AD cases in basal IRS-2 pS.

Supplemental Table 3A

Basal and insulin-stimulated levels of signaling molecules and their interactions in the hippocampal formation of normal (N) and AD cases[A]

Signaling molecule ratios	0 nM Insulin (Basal Levels)			1 nM Insulin			10 nM Insulin		
	N	AD	N vs. AD *P* Value	N	AD	N vs. AD *P* Value	N	AD	N vs. AD *P* Value
IR									
IR $pY^{1150/1151}$/ IRβ	0.14 ± 0.01	0.11 ± 0.01	0.10031	0.80 ± 0.11	0.48 ± 0.03	0.01092	1.01 ± 0.12	0.69 ± 0.04	<0.00001
IR pY^{960}/ IRβ	0.15 ± 0.01	0.13 ± 0.01	0.14113	0.61 ± 0.06	0.38 ± 0.01	0.02504	0.81 ± 0.02	0.56 ± 0.02	0.01993
IGF-1R									
IGF-1 $pY^{1135/1136}$/ IGF-1β	0.24 ± 0.02	0.20 ± 0.02	0.14369	0.32 ± 0.05	0.25 ± 0.03	0.18216	0.72 ± 0.09	0.43 ± 0.06	0.00652
IRS-1									
Total IRS-1 pY/ IRS-1	0.10 ± 0.02	0.25 ± 0.02	0.00064	0.39 ± 0.03	0.29 ± 0.03	0.01072	0.48 ± 0.06	0.34 ± 0.02	0.02394
IRS-1 pY^{612}/ IRS-1	0.10 ± 0.01	0.24 ± 0.02	0.00091	0.30 ± 0.02	0.30 ± 0.01	0.74991	0.41 ± 0.02	0.32 ± 0.01	0.00060
Total IRS-1 pS/ IRS-1	0.14 ± 0.01	0.28 ± 0.02	0.00026	0.46 ± 0.04	0.30 ± 0.02	0.00582	0.56 ± 0.04	0.36 ± 0.03	<0.00001
IRS-1 pS^{312}/ IRS-1	0.13 ± 0.01	0.22 ± 0.01	0.00050	0.31 ± 0.02	0.60 ± 0.04	0.00020	0.45 ± 0.03	0.77 ± 0.04	<0.00001
IRS-1 pS^{616}/ IRS-1	0.16 ± 0.02	0.32 ± 0.03	<0.00001	0.38 ± 0.03	0.37 ± 0.03	0.58613	0.53 ± 0.05	0.44 ± 0.04	0.03392
IRS-1 $pS^{636/639}$/ IRS-1	0.09 ± 0.01	0.14 ± 0.01	0.01102	0.25 ± 0.02	0.40 ± 0.02	0.00022	0.31 ± 0.01	0.52 ± 0.02	<0.00001
IRS-1 interactions									
IRS-1 bound to IRβ/ IRβ	0.04 ± 0.01	0.05 ± 0.01	0.43973	0.35 ± 0.04	0.23 ± 0.02	0.01501	0.43 ± 0.02	0.31 ± 0.02	0.00044
IRS-1 bound to IGF-1Rβ/ IGF-1Rβ	0.05 ± 0.01	0.04 ± 0.01	0.56314	0.10 ± 0.02	0.09 ± 0.03	0.44015	0.35 ± 0.03	0.16 ± 0.03	<0.00001
PI3K p85α bound to IRS-1/ IRS-1	0.10 ± 0.01	0.27 ± 0.03	0.00080	0.32 ± 0.03	0.29 ± 0.03	0.04731	0.41 ± 0.04	0.36 ± 0.05	0.00243
IRS-2									
Total IRS-2 pY/ IRS-2	0.07 ± 0.01	0.14 ± 0.01	0.00013	0.10 ± 0.01	0.15 ± 0.02	0.01335[B]	0.20 ± 0.02	0.17 ± 0.01	0.23490
Total IRS-2 pS/ IRS-2	0.12 ± 0.01	0.25 ± 0.03	0.00139	0.20 ± 0.04	0.28 ± 0.03	0.19953	0.39 ± 0.02	0.35 ± 0.03	0.44023
IRS-2 interactions									
IRS-2 bound to IRβ/ IRβ	0.04 ± 0.02	0.04 ± 0.02	0.73374	0.05 ± 0.02	0.04 ± 0.02	0.19151	0.06 ± 0.02	0.05 ± 0.02	0.80450
PI3K p85α bound to IRS-2/ IRS-2	0.14 ± 0.01	0.25 ± 0.02	<0.00001	0.18 ± 0.03	0.26 ± 0.02	0.02913[B]	0.34 ± 0.02	0.30 ± 0.02	0.07577

[A]Data expressed as ratios (mean ± S.E.M) of signaling molecules listed at left, either levels of a phosphorylated molecule to total levels of that molecule or levels of a bound molecule to total levels of the molecule to which it is bound. 1 nM insulin selectively activates the IR, but 10 nM insulin activates the IR and IGF-1R (see text Figures 1 and 2 and Supplemental Figures 2 and 3).

[B]Although there were significant between-groups (N vs. AD) effects on levels of IRS-2 pY at 1 nM insulin, that dose did not significantly increase values above baseline levels within either diagnostic group. The between-groups effect thus appears to reflect differences between N and AD cases in basal IRS-2 pY.

Supplemental Table 3B

Basal and insulin-stimulated levels of downstream signaling molecules in the hippocampal formation of normal (N) and AD cases[A]

Signaling molecule ratios	0 nM Insulin (Basal Levels)			1 nM Insulin			10 nM Insulin		
	N	AD	N vs. AD *P* Value	N	AD	N vs. AD *P* Value	N	AD	N vs. AD *P* Value
Akt1									
Akt1 pS^{473}/ Akt1	0.11 ± 0.02	0.34 ± 0.02	<0.00001	0.48 ± 0.03	0.46 ± 0.03	0.5652	0.63 ± 0.04	0.53 ± 0.08	0.00071
GSK-3β									
GSK-3β pY^{216}/ GSK-3β	0.46 ± 0.04	0.32 ± 0.04	0.00782	0.61 ± 0.06	0.38 ± 0.01	0.5055	0.23 ± 0.03	0.28 ± 0.05	0.37605
GSK-3β pS^{9}/ GSK-3β	0.18 ± 0.02	0.20 ± 0.03	0.25830	0.54 ± 0.09	0.27 ± 0.05	0.0293	0.84 ± 0.09	0.49 ± 0.04	0.00944
mTOR									
mTOR pS^{2448}/ mTOR	0.10 ± 0.02	0.20 ± 0.03	0.00081	0.45 ± 0.02	0.38 ± 0.03	0.0502	0.57 ± 0.02	0.42 ± 0.04	0.00525
ERK2									
ERK2 pT^{185}/pY^{187}/ ERK2	0.07 ± 0.01	0.19 ± 0.02	0.00033	0.38 ± 0.03	0.26 ± 0.03	0.0159	0.54 ± 0.04	0.31 ± 0.01	0.00011

[A]Data expressed as ratios (mean ± S.E.M) of signaling molecules listed at left, specifically levels of a phosphorylated molecule to total levels of that molecule. 1 nM insulin selectively activates the IR, but 10 nM insulin activates the IR and IGF-1R (see text Figures 1 and 2 and Supplemental Figures 2 and 3).

Supplemental Table 4

Basal and IGF-1-stimulated levels of signaling molecules and their interactions in cerebellar cortex of normal (N) and AD cases[A]

Signaling molecule ratios	0 nM IGF-1 (Basal Levels)			1 nM IGF-1			10 nM IGF-1		
	N	AD	N vs. AD *P* Value	N	AD	N vs. AD *P* Value	N	AD	N vs. AD *P* Value
IGF-1R									
IGF-1R pY$^{1135/1136}$/ IGF-1R	0.25 ± 0.03	0.27 ± 0.03	0.72098	0.57 ± 0.06	0.42 ± 0.03	0.04453	0.93 ± 0.11	0.60 ± 0.12	0.03087
IGF-1R pY^{1131}/ IGF-1R	0.12 ± 0.01	0.13 ± 0.02	0.50077	0.38 ± 0.04	0.20 ± 0.03	0.01189	0.54 ± 0.04	0.36 ± 0.05	0.01094
IRS-1									
Total IRS-1 pY/ IRS-1	0.20 ± 0.02	0.21 ± 0.01	0.74941	0.24 ± 0.02	0.23 ± 0.02	0.68220	0.32 ± 0.03	0.26 ± 0.02	0.15413
Total IRS-1 pS/ IRS-1	0.21 ± 0.02	0.23 ± 0.02	0.39241	0.27 ± 0.02	0.27 ± 0.03	0.57407	0.29 ± 0.03	0.31 ± 0.03	0.47167
IRS-1 interactions									
IRS-1 bound to IRβ/ IRβ	0.12 ± 0.02	0.13 ± 0.03	0.76761	0.15 ± 0.03	0.15 ± 0.02	0.50151	0.31 ± 0.03	0.19 ± 0.02	0.00142
IRS-1 bound to IGF-1Rβ/ IGF-1Rβ	0.03 ± 0.01	0.03 ± 0.01	0.60944	0.03 ± 0.01	0.03 ± 0.02	0.55929	0.03 ± 0.01	0.02 ± 0.01	0.23080
PI3K p85α bound to IRS-1/ IRS-1	0.25 ± 0.01	0.29 ± 0.03	0.13070	0.30 ± 0.02	0.33 ± 0.04	0.28751	0.36 ± 0.02	0.38 ± 0.05	0.41547
IRS-2									
Total IRS-2 pY/ IRS-2	0.09 ± 0.01	0.11 ± 0.01	0.19324	0.32 ± 0.02	0.17 ± 0.02	0.01586	0.46 ± 0.03	0.28 ± 0.03	0.00027
Total IRS-2 pS/ IRS-2	0.07 ± 0.01	0.13 ± 0.01	0.00320	0.24 ± 0.02	0.18 ± 0.01	0.02997	0.34 ± 0.03	0.27 ± 0.02	0.04437
IRS-2 interactions									
IRS-2 bound to IGF-1Rβ/ IGF-1Rβ	0.10 ± 0.01	0.14 ± 0.03	0.19132	0.35 ± 0.03	0.22 ± 0.03	0.00373	0.48 ± 0.03	0.32 ± 0.04	0.01095
PI3K p85α bound to IRS-2/ IRS-2	0.09 ± 0.01	0.10 ± 0.01	0.48043	0.35 ± 0.02	0.23 ± 0.04	0.01539	0.51 ± 0.03	0.35 ± 0.03	0.00220

[A]Data expressed as ratios (mean ± S.E.M) of signaling molecules listed at left, either levels of a phosphorylated molecule to total levels of that molecule or levels of a bound molecule to total levels of the molecule to which it is bound. 1 nM IGF-1 selectively activates the IGF-1R, but 10 nM IGF-1 activates IGF-1R and the IR (see text Figures 1 and 2 and Supplemental Figures 2 and 3).

Supplemental Table 5

Basal and IGF-1-stimulated levels of signaling molecules and their interactions in the hippocampal formation of normal (N) and AD cases[A]

Signaling molecule ratios	0 nM IGF-1 (Basal Levels)			1 nM IGF-1			10 nM IGF-1		
	N	AD	N vs. AD *P* Value	N	AD	N vs. AD *P* Value	N	AD	N vs. AD *P* Value
IGF-1R									
IGF-1R $pY^{1135/1136}$/ IGF-1R	0.17 ± 0.02	0.19 ± 0.02	0.30320	0.46 ± 0.03	0.22 ± 0.02	<0.00001	0.69 ± 0.06	0.39 ± 0.07	0.00393
IGF-1R pY^{1131}/ IGF-1R	0.15 ± 0.01	0.19 ± 0.02	0.07011	0.45 ± 0.02	0.27 ± 0.02	<0.00001	0.66 ± 0.04	0.31 ± 0.02	<0.00001
IR									
IR $pY^{1150/1151}$/ IR	0.22 ± 0.02	0.24 ± 0.02	0.94184	0.24 ± 0.02	0.24 ± 0.02	0.91998	0.56 ± 0.04	0.34 ± 0.05	0.00125
IR pY^{960}/ IR	0.15 ± 0.02	0.18 ± 0.02	0.29355	0.16 ± 0.02	0.19 ± 0.02	0.20104	0.47 ± 0.04	0.27 ± 0.04	0.00117
IRS-1									
Total IRS-1 pY/ IRS-1	0.12 ± 0.01	0.24 ± 0.02	<0.00001	0.15 ± 0.01	0.25 ± 0.02	<0.00001[B]	0.25 ± 0.02	0.26 ± 0.02	0.36759
Total IRS-1 pS/ IRS-1	0.17 ± 0.02	0.28 ± 0.02	<0.00001	0.19 ± 0.02	0.30 ± 0.02	0.00018[B]	0.31 ± 0.02	0.32 ± 0.02	0.91739
IRS-1 interactions									
IRS-1 bound to IRβ/ IRβ	0.13 ± 0.02	0.13 ± 0.02	0.92747	0.14 ± 0.01	0.16 ± 0.02	0.84931	0.33 ± 0.02	0.21 ± 0.03	0.00162
IRS-1 bound to IGF-1Rβ/ IGF-1Rβ	0.04 ± 0.01	0.04 ± 0.02	0.96267	0.04 ± 0.01	0.05 ± 0.02	0.70993	0.05 ± 0.01	0.05 ± 0.02	0.80955
PI3K p85α bound to IRS-1/ IRS-1	0.16 ± 0.02	0.31 ± 0.02	<0.00001	0.19 ± 0.02	0.33 ± 0.02	<0.00001	0.28 ± 0.02	0.34 ± 0.03	0.41547
IRS-2									
Total IRS-2 pY/ IRS-2	0.10 ± 0.01	0.20 ± 0.02	<0.00001	0.35 ± 0.02	0.23 ± 0.02	0.00065	0.41 ± 0.04	0.30 ± 0.02	0.00695
Total IRS-2 pS/ IRS-2	0.11 ± 0.01	0.23 ± 0.02	<0.00001	0.40 ± 0.05	0.26 ± 0.02	0.02256	0.54 ± 0.05	0.32 ± 0.04	0.00222
IRS-2 interactions									
IRS-2 bound to IGF-1Rβ/ IGF-1Rβ	0.09 ± 0.01	0.12 ± 0.02	0.13927	0.34 ± 0.03	0.16 ± 0.02	0.00057	0.47 ± 0.04	0.23 ± 0.03	<0.00001
PI3K p85α bound to IRS-2/ IRS-2	0.15 ± 0.02	0.32 ± 0.03	<0.00001	0.45 ± 0.04	0.35 ± 0.02	0.04606	0.56 ± 0.05	0.43 ± 0.03	0.04169

[A]Data expressed as ratios (mean ± S.E.M) of signaling molecules listed at left, either levels of a phosphorylated molecule to total levels of that molecule or levels of a bound molecule to total levels of the molecule to which it is bound. 1 nM IGF-1 selectively activates the IGF-1R, but 10 nM IGF-1 activates IGF-1R and the IR (see text Figures 1 and 2 and Supplemental Figures 2 and 3).

[B]Although there were significant between-groups (N vs. AD) effects on IRS-1 pY and pS at 1 nM IGF-1, that dose did not significantly increase values above baseline levels within either diagnostic group. The between-groups effect thus appears to reflect differences between N and AD cases in basal IRS-1 pY and pS.

Supplemental Table 6 (cont'd on next page)

Antibodies and reaction conditions used for immunohistochemistry

Antigen	Antibody (Ab)	Ab Type[A]	Ab Dilution	Epitope Retrieval Method[B]	Signal Amplification Method[C]
Aβ (amyloid beta), total (NAB228)	Santa Cruz 32277	Ms mAb	1:500	FA	$NiSO_4$
Aβ oligomers (1)	NAB61	Ms mAb	1:500	FA	$NiSO_4$
Aβ oligomers (2)	NU-1[D]	Ms mAb	1:1000	FA	$NiSO_4$
Aβ oligomers (3)	NU-4[D]	Ms mAb	1:1000	FA	$NiSO_4$
Akt (= PKB, Protein Kinase B)	Rockland 100-401	Rb pAb	1:2000	HIER/EDTA	TSA
Akt1 pS^{473}	Cell Signaling 4051	Ms mAb	1:300	HIER/EDTA	TSA
Akt2 pS^{474}	Abcam 38513	Rb pAb	1:300	HIER/EDTA	TSA
AS160 (Akt Substrate, 160 kDa) pT^{642}	Invitrogen 44-1071G	Rb pAb	1:100	HIER/EDTA	$NiSO_4$
Glucose transporter 4 (GLUT4) pS^{488}	Santa Cruz 17558	Rb pAb	1:100	HIER/EDTA	$NiSO_4$
GSK-3β (Glycogen synthase kinase-3β)	Cell Signaling 9315	Rb mAb	1:50	HIER/EDTA	$NiSO_4$
GSK-3α/β $pS^{21/9}$	Cell Signaling 9331	Rb pAb	1:300	HIER/EDTA	TSA
IKK (Inhibitor of κB Kinase) α/β $pS^{176/180}$	Cell Signaling 2697	Rb mAb	1:100	HIER/EDTA	$NiSO_4$
IRβ (Insulin Receptor, Beta Chain)	Santa Cruz 711	Rb pAb	1:100	HIER/EDTA	$NiSO_4$
IRβ pY^{960}	Invitrogen 44-800G	Rb pAb	1:100	Trypsin	$NiSO_4$
IRβ $pY^{1150/1151}$/IGF-1Rβ $pY^{1135/1136}$	Invitrogen 44-804	Rb pAb	1:100	Trypsin	$NiSO_4$
IRS-1 (Insulin Receptor Substrate-1)	Santa Cruz 7200	Rb pAb	1:100	HIER/EDTA	$NiSO_4$
IRS-1 pS^{312}	Invitrogen 44-814G	Rb pAb	1:100	HIER/EDTA	$NiSO_4$
IRS-1 pS^{616}	Invitrogen 44-550G	Rb pAb	1:500	HIER/EDTA	$NiSO_4$
IRS-1 $pS^{636/639}$	Cell Signaling 2388	Rb pAb	1:100	HIER/EDTA	$NiSO_4$
IRS-1 pY^{612}	Invitrogen 44-816G	Rb pAb	1:100	HIER/EDTA	$NiSO_4$
IRS-1 pY^{941}	Invitrogen 44-820G	Rb pAb	1:800	HIER/EDTA	$NiSO_4$
JNK (c-Jun N-terminal Kinase) 1+2 pT^{183}/pY^{185}	Invitrogen 44-682G	Rb pAb	1:100	HIER/EDTA	$NiSO_4$
mTOR (mammalian Target of Rapamycin = FRAP1) pS^{2448}	Cell Signaling 2976	Rb mAb	1:50	HIER/EDTA	$NiSO_4$
Nitrotyrosine	Millipore MAB 5404	Ms mAb	1:100	HIER/EDTA	$NiSO_4$
PIP3 (Phosphatidyl inositol [3,4,5] P3)	Echelon Z-P345b	Ms mAb	1:10,000	HIER/EDTA	Silver-Gold
PKC (Protein Kinase C) ζ/λ $pT^{410/403}$	Cell Signaling 9378	Rb pAb	1:50	HIER/EDTA	$NiSO_4$

Supplemental Table 6 (cont'd)

Antibodies and reaction conditions used for immunohistochemistry

Antigen	Antibody (Ab)	Ab Type[A]	Ab Dilution	Epitope Retrieval Method[B]	Signal Amplification Method[C]
PP2A (Protein Phosphatase, type 2A), catalytic subunit	BD Biosci. 610555	Ms mAb	1:1500	HIER/EDTA	$NiSO_4$
PP2B (Protein Phosphatase, type 2B = Calcineurin), α-subunit	Sigma C1956	Ms mAb	1:2000	HIER/EDTA	$NiSO_4$
PTEN (Phosphatase and Tensin homolog)	Cell Signaling 9559	Rb mAb	1:500	HIER/EDTA	TSA
PTP1B (Prot. Tyrosine Phosphatase 1B)	BD Biosci. 610139	Ms mAb	1:100	HIER/EDTA	$NiSO_4$
Tau pS^{202}/pT^{205}	Thermo Sci. AT8	Ms mAb	1:800	FA	$NiSO_4$

[A] mAb = monoclonal antibody, pAb = polyclonal antibody, Ms = mouse, Rb = rabbit

[B] FA = immersion in 88% formic acid for 5 min

HIER = heat-induced epitope retrieval in 10 mM citrate, pH 6.0 or 1 mM EDTA, pH 8.0 for 10 min

Trypsin = exposure to dissolved trypsin tablets (Sigma T-7168) at 30°C for 20 min

[C] $NiSO_4$ = nickel sulfate added to DAB solution

Silver-gold = intensification of DAB reaction product with silver nitrate and gold toning

TSA = tyramide signal amplification (PerkinElmer SAT700)

[D] Generously supplied by William L. Klein (Northwestern University)

(Supplemental Tables 7-9 on the following pages)

Supplemental Table 7

Correlations of activated IRS-1 kinases with Aβ plaque load and neurofibrillary tangle density in CA1[A]

IRS-1 Kinase[B]	Total Aβ Plaque Load[C]			Oligomeric Aβ Plaque Load[D]			NFT Density[E]		
	r	t (df)	*p* value	r	t (df)	*p* value	r	t (df)	*p* value
IKKα/β $pS^{176/180}$	0.3009	2.91 (85)	0.00461	0.3148	2.98 (81)	0.00380	0.2975	2.79 (80)	0.00659
JNK 1/2 pT^{183}/pY^{185}	0.2594	2.48 (85)	0.01511	0.4483	4.49 (80)	0.00002	0.4695	4.73 (79)	0.00001
mTOR pS^{2448}	0.1474	1.39 (87)	0.16808	0.3069	2.94 (83)	0.00425	0.2861	2.70 (82)	0.00842
PKC ζ/λ $pT^{410/403}$	0.3367	3.24 (82)	0.00173	0.4453	4.39 (78)	0.00004	0.5396	5.62 (77)	$<1x10^{-6}$
Comparison Variables									
Akt1 pS^{473}	0.2766	2.25 (61)	0.02807	0.3482	2.85 (59)	0.00601	0.3621	2.98 (59)	0.00418
Akt2 pS^{474}	-0.0094	-0.08 (65)	0.93648	-0.0302	-0.24 (61)	0.81114	0.1359	1.08 (62)	0.28432
GSK-3α/β $pS^{21/9}$	0.3470	2.91 (62)	0.00501	0.4483	3.92 (61)	0.00023	0.4360	3.75 (62)	0.00400
Nitrotyrosine	0.2082	1.81 (72)	0.07447	0.2761	2.39 (69)	0.01958	0.2744	2.34 (67)	0.02227

[A]Based on combined data from normal, MCI, and AD cases in the ROS cohort. Very similar results were obtained on combined data from normal and AD cases in the UPenn cohort. Measures used to quantify levels of the antigens listed are specified in text Table 5. Variability in number of cases studied for each antigen, evident in the degrees of freedom (df), reflect differences in tissue availability, tissue integrity, and/or signal detection problems in some sections.

[B]While GSK-3 is an IRS-1 serine kinase, it is listed as a comparison variable because it is not known to directly phosphorylate IRS-1 at the sites studied (S312, S616, and S636/639) and because we lack qIHC data only on its activated form. By an unknown mechanism, however, GSK-3 can promote phosphorylation of IRS-1 at S312 (= S307 in rodents) (39).

[C]As determined with NAB228.

[D]As determined with NU-4. Similar results for oAβ were obtained with NU-1 and NAB61.

[E]NFT = neurofibrillary tangle

Supplemental Table 8

Antibodies used for immunoprecipitation

Antigen	Antibody (Ab)	Ab Type	Ab/200 ug Lysate
Akt1	Santa Cruz 5298	Mouse mAb	1.2 μg
AS160	Cell Signaling 2447	Rabbit pAb	1.0 μg
ERK2	Santa Cruz 154	Rabbit pAb	1.0 μg
GLUT4	Santa Cruz 7938	Rabbit pAb	1.0 μg
GSK-3β	Santa Cruz 8257	Goat pAb	1.0 μg
IRβ	Santa Cruz 20739	Rabbit pAb	1.0 μg
IGF-1Rβ	Santa Cruz 9038	Rabbit pAb	1.0 μg
IRS-1	Cell Signaling 2382	Rabbit pAb	1.0 μg
IRS-2	Santa Cruz 1555	Goat pAb	1.2 μg
mTOR	Santa Cruz 1550-R	Rabbit pAb	1.5 μg

Supplemental Table 9

Antibodies used for immunoblotting

Antigen	Antibody (Ab)	Ab Type	Ab Dilution
Akt1-3	Santa Cruz 8312	Rabbit pAb	1:500
Akt1-3 pS^{473}	Santa Cruz 7985-R	Rabbit pAb	1:500
AS160	Cell Signaling 2447	Rabbit mAb	1:1000
AS160 pT^{642}	Invitrogen 44-1071G	Rabbit pAb	1:1000
ERK2	Santa Cruz 154	Rabbit pAb	1:500
ERK2 pT^{183}/pY^{185}	Santa Cruz 81492	Mouse mAb	1:500
GLUT4	Santa Cruz 53566	Mouse mAb	1:750
GLUT4 pS^{488}	Santa Cruz 17558	Goat pAb	1:750
GSK-3β	Santa Cruz 53931	Mouse mAb	1:500
GSK-3β pS^{9}	Cell Signaling 9322	Rabbit mAb	1:500
GSK-3β pY^{216}	Santa Cruz 135653	Rabbit pAb	1:750
IRβ	Santa Cruz 81465	Mouse mAb	1:500
IRβ pY^{960}	Invitrogen 44-800G	Rabbit pAb	1:1000
IRβ $pY^{1150/1151}$/IGF-1Rβ $pY^{1135/1136}$	Invitrogen 44-804G	Rabbit pAb	1:1000
IRβ pY^{1146}/IGF-1Rβ pY^{1131}	Cell Signaling 3021	Rabbit mAb	1:750
IGF-1Rβ	Santa Cruz 81167	Mouse mAb	1:750
IRS-1	Santa Cruz 8038	Mouse mAb	1:750
IRS-1 pS^{312}	Invitrogen 44-814G	Rabbit pAb	1:1000
IRS-1 pS^{616}	Invitrogen 44-550G	Rabbit pAb	1:1000
IRS-1 $pS^{636/639}$	Cell Signaling 2388	Rabbit pAb	1:1000
IRS-1 pY^{612}	Invitrogen 44-816G	Rabbit pAb	1:1000
IRS-2	Santa Cruz 8299	Rabbit pAb	1:500
mTOR	Santa Cruz 136269	Mouse mAb	1:500
mTOR pS^{2448}	Cell Signaling 2971	Rabbit pAb	1:1000
Phosphoserine	Santa Cruz 81516	Mouse mAb	1:500
Phosphotyrosine	Santa Cruz 508	Mouse mAb	1:750
PI3K p85α	Santa Cruz 71896	Mouse mAb	1 :750

Supplemental References

1. Bennett DA, Schneider JA, Bienias JL, Evans DA, Wilson RS. Mild cognitive impairment is related to Alzheimer disease pathology and cerebral infarctions. *Neurology* 2005;64(5):834-841.
2. Bennett DA, et al. Natural history of mild cognitive impairment in older persons. *Neurology* 2002;59(2):198-205.

3. McKhann G, et al. Clinical diagnosis of Alzheimer's disease: report of the NINCDS-ADRDA Work Group under the auspices of Department of Health and Human Services Task Force on Alzheimer's Disease. *Neurology* 1984;34(7):939-944.
4. Mirra SS, et al. The Consortium to Establish a Registry for Alzheimer's Disease (CERAD). Part II. Standardization of the neuropathologic assessment of Alzheimer's disease. *Neurology* 1991;41(4):479-486.
5. Hyman BT, Trojanowski JQ. Editorial on consensus recommendations for the postmortem diagnosis of Alzheimer disease from the National Institute on Aging and the Reagan Institute working group on diagnostic criteria for the neuropathological assessment of Alzheimer disease. *J Neuropathol Exp Neurol.* 1997;56(10):1095-1097.
6. Nelson AP, O'Connor, MG. Mild cognitive impairment: a neuropsychological perspective. *CNS Spectr.* 2008;13(1):56-64.
7. Petersen RC, Negash S. Mild cognitive impairment: an overview. *CNS Spectr.* 2008;13(1):45-53.
8. Wilson RS, et al. Individual differences in rates of change in cognitive abilities of older persons. *Psychol Aging* 2002;17(2):179-193.
9. Wilson RS, et al. Participation in cognitively stimulating activities and risk of incident Alzheimer disease. *JAMA* 2002;287(6):742-748.
10. Maddox PH, Jenkins D. 3-Aminopropyltriethoxysilane (APES): a new advance in section adhesion. *J Clin Pathol.* 1987;40(10):1256-1260.
11. Kitamoto, T., Ogomori, K., Tateishi, J., and Prusiner, S.B. Formic acid pretreatment enhances immunostaining of cerebral and systemic amyloids. *Lab Invest.* 1987; 57(2):230-236.
12. Pileri SA, et al. Antigen retrieval techniques in immunohistochemistry: comparison of different methods. *J Pathol.* 1997;183(1):116-123.
13. Scopsi L, Larsson LI. Increased sensitivity in peroxidase immunocytochemistry. A comparative study of a number of peroxidase visualization methods employing a model system. *Histochemistry* 1986;84(3):221-230.
14. Teclemariam-Mesbah R, Wortel J, Romijn HJ, Buijs RM . A simple silver-gold intensification procedure for double DAB labeling studies in electron microscopy. *J Histochem Cytochem* 1997;45(4):619-621.
15. Soetanto A, et al. Association of anxiety and depression with microtubule-associated protein 2- and synaptopodin-immunolabeled dendrite and spine densities in hippocampal CA3 of older humans. *Arch Gen Psychiatry* 2010;67(5):448-457.
16. Sesti G. Pathophysiology of insulin resistance. *Best Pract Res Clin Endocrinol Metab.* 2006;20(4):665-679.
17. Boura-Halfon S, Zick Y. Phosphorylation of IRS proteins, insulin action, and insulin resistance. *Am J Physiol Endocrinol Metab.* 2009;296(4):E581-591.
18. Boura-Halfon S, Zick Y. Serine kinases of insulin receptor substrate proteins. *Vitam Horm.* 2009;80:313-349.
19. Fröjdö S, Vidal H, Pirola L. Alterations of insulin signaling in type 2 diabetes: a review of the current evidence from humans. *Biochim Biophys Acta* 2009;1792(2):83-92.
20. Abdul-Ghani MA, DeFronzo RA. Pathogenesis of insulin resistance in skeletal muscle. *J Biomed Biotechnol.* 2010;476279.
21. Yip CC, Moule ML, Yeung CW. Characterization of insulin receptor subunits in brain and other tissues by photoaffinity labeling. *Biochem Biophys Res Commun.* 1980;96(4):1671-1678.
22. Heidenreich KA, Zahniser NR, Berhanu P, Brandenburg D, Olefsky JM. Structural differences between insulin receptors in the brain and peripheral target tissues. *J Biol Chem.* 1983;258(14):8527-8530.

23. Gammeltoft S, Fehlmann M, van Obberghen, E. Insulin receptors in the mammalian central nervous system: binding characteristics and subunit structure. *Biochimie* 1985;67(10-11):1147-1153.
24. Seino S, Bell GI. Alternative splicing of human insulin receptor messenger RNA. *Biochem Biophys Res Commun.* 1989;159(1):312-316.
25. Cheatham B, Kahn CR. Insulin action and the insulin signaling network. *Endocr Rev.* 1995;16(2):117-142.
26. Combettes-Souverain M, Isaad T. Molecular basis of insulin action. *Diabetes Metabol.* 1999;24:477-489.
27. Hirai T, Chida K. Protein kinase Cζ(PKCζ): activation mechanisms and cellular functions. *J Biochem.* 2003;133(1):1-7.
28. Sale EM, Sale GJ. Protein kinase B: signalling roles and therapeutic targeting. *Cell Mol Life Sci.* 2008;65(1):113-127.
29. Zhande R, et al. Dephosphorylation by default, a potential mechanism for regulation of insulin receptor substrate-1/2, Akt, and ERK1/2. *J Biol Chem.* 2006;281(51):39071-39080.
30. Morisco C, et al. Akt mediates the cross-talk between beta-adrenergic and insulin receptors in neonatal cardiomyocytes. *Circ Res.* 2005;96(2):180-188.
31. Sun XJ, Liu F. Phosphorylation of IRS proteins: yin-yang regulation of insulin signaling. *Vitam Horm.* 2009; 80:351-387.
32. Veilleux A, Houde VP, Bellmann K, Marette A. Chronic inhibition of the mTORC1/S6K1 pathway increases insulin-induced PI3K activity but inhibits Akt2 and glucose transport stimulation in 3T3-L1 adipocytes. *Mol Endocrinol.* 2010;24(4):766-778.
33. Moeschel K, et al. Protein kinase C-ζ-induced phosphorylation of Ser318 in insulin receptor substrate-1 (IRS-1) attenuates the interaction with the insulin receptor and the tyrosine phosphorylation of IRS-1. *J Biol Chem.* 2004; 279(24):25157-25163.
34. Liberman Z, Eldar-Finkelman H. Serine 332 phosphorylation of insulin receptor substrate-1 by glycogen synthase kinase-3 attenuates insulin signaling. *J Biol Chem.* 2005;280(6):4422-4428.
35. Yi Z, Luo M, Carroll CA, Weintraub ST, Mandarino LJ. Identification of phosphorylation sites in insulin receptor substrate-1 by hypothesis-driven high-performance liquid chromatography-electrospray ionization tandem mass spectrometry. *Anal Chem.* 2005;77(17):5693-5699.
36. Stretton C, Evans A, Hundal HS. Cellular depletion of atypical PKCλ is associated with enhanced insulin sensitivity and glucose uptake in L6 rat skeletal muscle cells. *Am J Physiol Endocrinol Metab.* 2010;299(3):E402-412.
37 Chong YH, et al. ERK1/2 activation mediates Aβ oligomer-induced neurotoxicity via caspase-3 activation and tau cleavage in rat organotypic hippocampal slice cultures. *J Biol Chem.* 2006;281(29):20315-20325.
38. Miscia S, et al. Aβ1-42 stimulated T cells express P-PKC-δ and P-PKC-ζ in Alzheimer disease. *Neurobiol Aging* 2009;30(3):394-406.
39. Henriksen EJ, Teachey MK. Short-term in vitro inhibition of glycogen synthase kinase 3 potentiates insulin signaling in type I skeletal muscle of Zucker diabetic fatty rats. *Metabolism Clin Exp.* 2007;56(7):931-938.